Veröffentlichung

Im Rahmen des SFB 880. www.sfb-880.tu-bs.de

Autoren: T. Beutel, N. Ferreira, M. Leester-Schädel, S. Büttgenbach

Titel: **Robust pressure sensor for measurements in boundary layers of liquid fluids with medium total pressures**

Journal, Seite, Verlag: n.a.

Konferenz, Ort: SPIE Microtechnologies, Proceedings of SPIE Vol. 8066

Jahr: 2011

Internet-Link (Doi-Nr.): http://dx.doi.org/10.1117/12.885610

Robust pressure sensor for measurements in boundary layers of liquid fluids with medium total pressures

T. Beutel*[1a], N. Ferreira[a], M. Leester-Schädel[a], S. Büttgenbach[a]
[a] Technische Universität Braunschweig, Institute for Microtechnology (IMT), Alte Salzdahlumer Straße 203, D-38124 Braunschweig, Germany

ABSTRACT

In this work, the latest results of the design, fabrication and characterization of a new MEMS piezoresistive pressure sensor are presented. It is made of silicon using a boron diffusion process to create piezoresistors. Significant changes in the layout as well as in the micro-fabrication process have been made, e.g. anodic bonding of a Pyrex cover on the backside. These lead to a very precise pressure sensor, which is tailor made for high dynamic measurements in fluids with a total pressure up to 4 *bar*. This new piezoresistive pressure sensor has been developed in order to meet the special requirements of measurements in fluid mechanics, particularly with regard to the non-intrusive nature of the sensor. The sensor development, starting with the simulation of mechanical stresses within the diaphragm is described. These calculations have lead to an optimized placement of the piezoresistors in order to achieve a maximum sensitivity. The result of this work is a sensor which has well known properties. Important parameters including sensitivity, resonance frequency and maximum load are described precisely. These are necessary to enable new measurements in the boundary layer of fluids. The experiments and the initial results, e.g. its linearity and its dynamic capability are demonstrated in several figures.

Keywords: piezoresistive pressure sensor, micro-fabrication, AeroMEMS, flow characterization, FEM simulation.

1. INTRODUCTION

Due to the ever increasing costs of energy, as well as aspects of environmental protection, ever more efficient products must be developed. In the aeronautical industry it is therefore necessary to continually investigate new concepts to reduce the fuel consumption and noise emission of civil aircraft. It is additionally important that airplane noise emissions during takeoff are extremely high and no longer accepted by the population. New models have therefore to be evaluated already in the development phase. The accelerated requirements of customers make these analyses even more important.

In a new approach to achieve high lift a coanda flap is used. By controlling suction and blow out of compressed air at discrete places along the wing shape, the drag is expected to be reduced significantly. The exhausted air is used to accelerate the near wall flow velocity above the coanda flap in order to maintain a laminar flow and generate a high lift coefficient C_L. This concept requires the ability to measure the state of the flow at high frequency and to be able to control it in real time. Current results of numerical investigations show that pulsed exhaust can produce similar performance to continuous flow with even less energy consumption, which is essential for a high over-all performance including all subsystems.

With new piezoceramic actuators, which make small changes to their length under high voltage excitation, it is possible to change the contour of wing sections. An oscillating lip enables pulsed blowing at the necessary frequency, by changing the height of the blowing slot. Novel sensor arrays are therefore required to enable time critical measurements of the flow conditions. These requirements have lead to the development of new sensors which are able to non-intrusively detect the state of the flow. Due to economic and technological reasons, it is advisable to use carbon fibre laminate as the wing's skin. We have shown that it is feasible to implement micro-fabricated sensors (AeroMEMS) flush to the fluid [1]. In this manuscript we describe the design and fabrication processes of second generation pressure sensors. All improvements are described precisely. Additionally, the initial measurement results are presented and discussed in the next subsection. Finally an outlook is provided.

[1] T.Beutel@TU-Braunschweig.de ; phone: +49 (0)531 391-9748 ; fax: +49 (0)531 391-9751 ; www.imt.tu-bs.de/

Smart Sensors, Actuators, and MEMS V, edited by Ulrich Schmid, José Luis Sánchez-Rojas, Monika Leester-Schaedel, Proc. of SPIE Vol. 8066, 80661U · © 2011 SPIE
CCC code: 0277-786X/11/$18 · doi: 10.1117/12.885610

2. SENSOR CONCEPT

In this section the reasons for a new sensor concept are explained. The boundary conditions set by the fabrication, the environmental conditions, the embedding process and the measurement purposes are described. At the end of each subsection the consequences for the sensor concept are summarized. This chapter leads to the design rules on which the sensor is based.

2.1 Basic geometry and limitations

This new approach to efficient active high lift requires the fabrication of a novel sensor. The main goal is to enable pressure and wall shear stress measurements at frequencies of at least $1\,kHz$ without disturbing the flow itself. Consequently the mounting of the sensors and actuators have to be flush to the wall. Therefore, it is a perfect solution to embed both into fibre composite material. This material is stiff enough to support the sensors and yet is flexible enough to change its contour for the actuator. Figure 1 shows the concept of the actuated lip in detail. The actuation enables high frequent changes of the slot height h. Because of a constant mass flow of pressurized air $\dot{m}$, the velocity V changes. This concept is expected to influence the flow above the coanda flap in the desired manner.

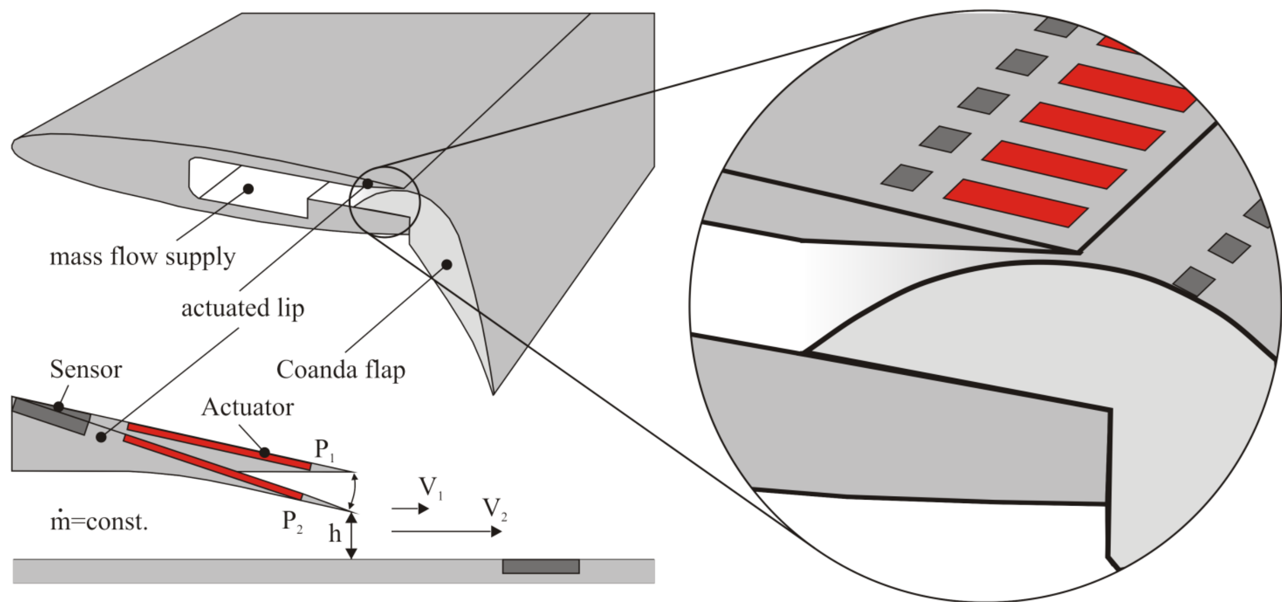

Figure 1: Scheme of the wing chord (top left) with a detailed drawing (right) of the sensor and actuator system placed over a coanda flap for active high lift. The actuator moves the lip between the positions P_1 and P_2, what results in the velocity V_1 and V_2 respectively (bottom left).

Because of the high demands on measuring frequency and accuracy, the first experiments will be performed in a water tunnel to reduce the control complexity of the system. Due to the high density of water, the needed system frequency is 10 times lower than in air. This simplifies the first steps in the experimental phase. In contrast, measuring in water with the micro-fabricated sensors will be a challenge. The pressure coefficient C_p over the entire airfoil was obtained from the project partners who conducted numerical experiments of the aerodynamic section. The maximum and minimum loads on the sensor are therefore able to be calculated.

In Figure 2 the principle of pressure measurement in the sensors is illustrated. In the left section, a sectional view of a 3D micro force sensor is shown. The characteristics of these have been published in [2] and were the basis of the investigations. In the first step, a new membrane shape which was adapted to the mechanical conditions (see section 2.4) was designed. The outer dimensions were then derived. The right section of Figure 2 shows the basic sensor geometry. The minimum dimensions are defined by the limitations of micro fabrication and by the maximum possible accuracy. The micro fabricated parts include the silicon pressure sensor and the Pyrex cover. The wiring is made of polyimide (PI) foil covered with a copper layer which was structured in house using a process similar to that for standard printed circuit boards (PCBs).

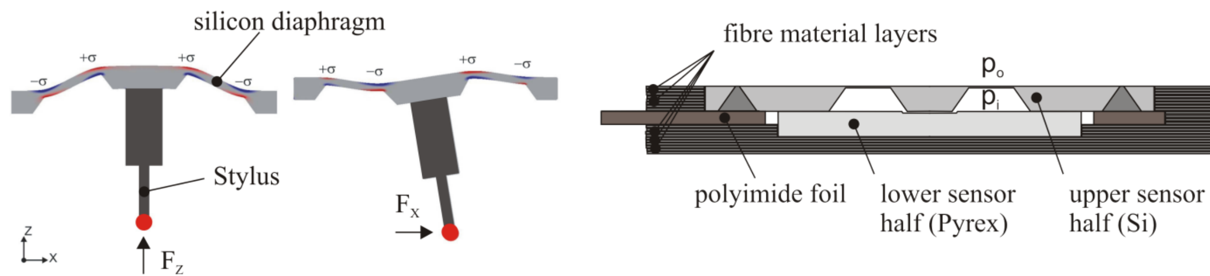

Figure 2: Comparison between 3-D micro force sensor (left, [2]) and the new concept of tailor-made pressure sensor embedded in fibre material (right).

Due to the reasons described in the introduction, the sensors have to measure two parameters. In addition to the pressure value, information about the wall shear stress is necessary to characterize the flow more exactly. For this reason another sensor will be integrated into the same chip, but here just the pressure sensor is described. The other sensor has no significant impact on the overall shape of the sensor modules.

2.2 State of the art

Based on literature research, the sensor presented is the first embedded into fibre material. The unique advantages of the extremely flush mounting in the wall offer many new possibilities.

Until now, most sensors have components which are exposed to the streaming fluid and are therefore intrusive. Often a variety of surface fences [3] or hot-wires [4] are used as the sensing element in the flow. As well as having the disadvantage of changing the flow, these components are very fragile and susceptible to damage from particles in the flow. These sensors are therefore only applied for scientific measurements in the laboratories. These sensors are also not likely suited for measurements in water.

The flush mounting of the sensor in the wall is a very important aspect of this sensor. Until now, many institutions have tried to design small sensors, which were later integrated into a model. The electrical connections were mostly placed downstream. In these cases, the sensor is placed flush within the wall, but the wiring not [3]. In this new approach, we integrate the sensors as well the necessary subsystems into the wall. This is a necessary step in order to be able to control the state of the flow. In other micro fabricated sensor projects, the creation of rounded contours was attempted. Very small sensors were designed and fabricated. In order to better represent a perfect curved geometry many small sensors were placed in close proximity to each other. This reduces the radius of curvature and allows smoother flow.

Flexible sensors based on flexible substrates have been the topic in many recent publications [5]. Hot-film sensors (e.g. by Tao of Systems Integration, Inc.) and pressure sensors have also been developed and are commercially available, but in very varying approaches.

In this approach, sensors are custom-made to be embedded into fibre composite material. This embedding process has extremely high demands on the sensor's capabilities, as illustrated in the following subsection. Since the embedding process is also being adapted for the integration of sensors, the concept seems to be feasible. Preliminary experiments with sensor dummies have been carried out in [1].

2.3 Embedding into fibre material

Before the embedding process, the sensor with the wiring is positioned in different layers of composite material. Because the sensor is much thicker than a single layer of composite material, each layer has areas which are cut to fit perfectly around the sensor. Figure 2 (right) shows a sectional view of the stack, which is mounted bottom up. The first fibre layers are uniform. Successive layers are cut out at the future sensor positions and layered to enable the placement of the Pyrex part of the sensor. The sensors are then mounted together with the wiring. Finally the last layer, which is cut to the shape of the silicon part of the sensor, is added. This step is the most critical, because the overall height has to fit perfectly to the sensors. The actuators can be mounted in the same way.

In the laminating process, a protective cover has to be placed above and below the stack. This cover has a special finish to prevent sticking. After placing the stack in an autoclave, a pressure of 0.3 *mbar* is drawn between the two protection layers so that no gas remains. A pressure of 3 *bar* is then applied outside the protection layer before the preheated resin is

pressed with 2.8 *bar* from one side to the other through the stack at 70°*C*. When all the resin is within the autoclave the in- and outflow is closed properly for the 12 *h* baking process at 120°*C*. After opening the autoclave and removing the protection layers the laminating process is finished.

During this process, the sensors are exposed to high mechanical and thermal loads. Additionally the duration of the process is a critical factor. The sensors were designed to withstand these loads, and in the initial experiments they were able to withstand the process. Currently, no sensor has been tested after the embedding process. Since the lamination process itself is part of the research the focus was on creating a planar surface. During the preliminary tests, either the sensors were dummies, or the wiring was not included.

2.4 Simulation of the membrane

The most crucial element of these doped silicon based sensors is the positioning of the piezoresistors on the diaphragm. The design of the membrane itself has a large impact on the maximum loads, the size and the measuring aspects e.g. linearity and resolution. Much effort is therefore necessary to develop a design, which has the desired properties and which is producible. In micro fabrication the limitations are given by the technologies which are available and by the type of wafer used.

As a starting point for design iteration, the force sensors shown in Figure 2 (left) were used. Because of the high pressures that must be measured (up to 4 *bar)*, the area of the diaphragm has to be reduced, or the thickness has to be increased. Both changes reduce the mechanical stress on the diaphragm. In order to stabilize the diaphragm, a boss structure is recommended. During the embedding process, it acts as a mechanical limiter for the maximum deflection of the membrane. The size of the compensation structures, which are necessary for anisotropic etching of (100)-silicon, leads to a minimum size of the membrane. Figure 3 shows the result of the simulation of the etching process for the sensor and the mask layout used for a wafer thickness of 360 μm. With the result of this simulation, which is the exact sensor geometry, the mechanical properties can be simulated using CosmosWorks®.

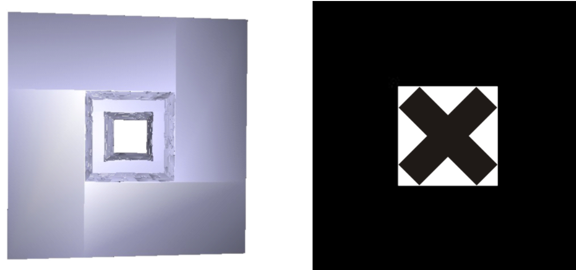

Figure 3: Screenshot of the etching result in the software tool SUZANA [6] (left) and the mask layout used for an etching process (see section 3) (right).

To determine the thickness of the membrane, all boundary conditions, and the safety factor adjusted maximum pressure have to be implemented in the simulation. Because of symmetry effects, only one quarter of the sensor needs to be simulated. This reduces the simulation time significantly. In this way it is possible to find an optimum thickness for the membrane.

The results of this simulation are shown in Figure 4 a). The membrane can withstand a pressure difference between p_o and p_i and the mechanical stresses on the surface are indicated by the colour b). The quantitative values of the stress are exported into an excel sheet in order to compute the optimum position of the piezoresistors on the membrane. As described before, this influences the accuracy significantly. In c) a plot of the numerical results is shown. The function $f(x)$ shows the mechanical stress [N/m^2] depending on the distance x to the centre of the membrane. In order to get a high sensitivity of the sensor, the piezoresistors have to be placed at the locations of high mechanical stress to obtain a high ΔR. The analytical expression for the change of the resistance is given by

$$\frac{\Delta R}{R} = \pi_L \sigma_L + \pi_T \sigma_T \tag{1}$$

where σ represents the mechanical stress in lateral (index L) or transversal (index T) directions to the current. π is the piezoresistive coefficient depending on the doping process and the wafer material and orientation. This cannot be manipulated during the design process.

As the geometry of the piezoresistors has been optimized in the past [2], the length *l* has been fixed at 200 μm, leading to a constant value of *R*. As shown in Figure 4 c) the mechanical stress σ is not constant. To find the optimal position for the centre of the resistors, the average stress over the length has to be maximised. The mathematical expression can be described as follows:

$$x_{opt,\sigma\max} = \left(\int_{x-\frac{1}{2}l}^{x+\frac{1}{2}l} \sigma(x)dx \right)_{\max} \tag{2}$$

In Figure 4 c) and d) the area of integration is represented, where it reaches its maximum. Hence, $x_{opt,\sigma max}$ is at the centre of this span. According to Figure 4 d) this position differs from the position of the maximum of σ(x).

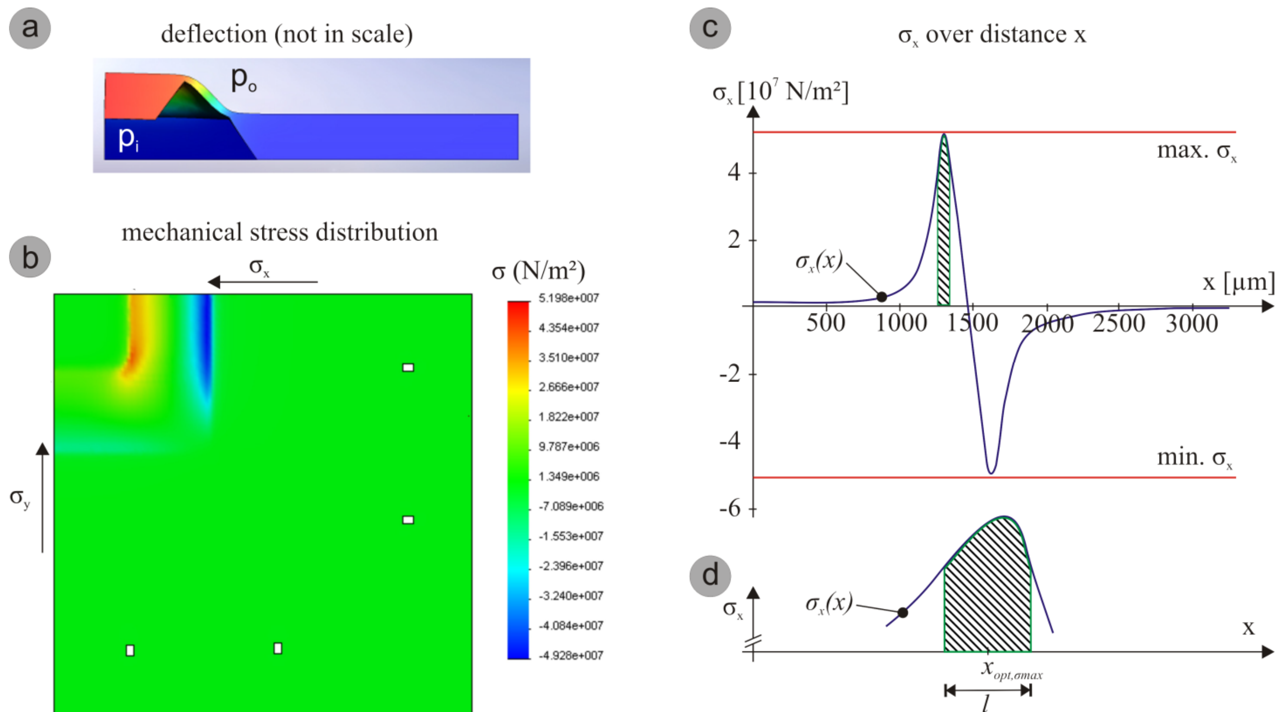

Figure 4: Simulation results of CosmosWorks® (left): a) shows the deflection of the membrane, while b) indicates the mechanical von-Mises-stress. The results of the simulation are shown in c) above for the half sensor. A detailed view including the description of *l* and $x_{opt,\sigma max}$ is presented in d).

The simulation results are only valid for the maximum pressure difference between p_i and p_o of 4 *bar*. They decrease if the pressure difference decreases. In [7] it has been demonstrated, that the values are also valid for a pressure difference of -4 *bar*, because the sensors' behaviour is reversible. The result of this simulation is an optimized membrane thickness of 45 μm and the value $\sigma_{max} \approx 5.5 \cdot 10^7\ N/m^2$. Also the feasibility of the wet-eching process has been proved and the sensitivity *S* can be roughly determined.

$$S = \frac{\Delta U_0}{U_i} \frac{1}{p_0} \approx \frac{\sigma(x_{opt,\sigma\max}) \cdot \pi}{p_{\max}} \frac{1}{U_i \cdot p_0} \approx 2{,}75 \frac{mV}{V \cdot bar} \tag{3}$$

Thereby the average value for π, which is known from measurements in the past, and $\sigma(x_{opt,\sigma max})$ were used.

3. SENSOR FABRICATION

3.1 Standard Fabrication process

The following fabrication process has been developed in order to realize the simulated design. The sensor has been fabricated on 4" Si wafers in a batch process using state of the art technologies. Up to now, the process was not completely carried out due to technical issues. The feasibility has been proved by several tests, in which various steps were completed independently. The first sensors were produced using steps 1 to 9, while the through-wafer connection was checked using steps 6-11. Figure 5 shows a simplified scheme of the most significant states during the process.

First, the diffusion of boron into the silicon substrate was used to fabricate the piezoresistors. For good ohmic contact, a highly doped "Pplus" area was added (2). Next, a Si_3N_4 layer is added as an etch stop layer for the through-wafer connections (3) before a SiO_2 is applied for electrical insulation (4). On the bottom side of the wafer, a SiO_2 and a Si_3N_4 layer were also deposited (5) to act as a second masking layer for wet-etching. The first masking layer was then structured (6) in order to allow advanced etching of 45 µm at the connection positions (7). The second masking layer is then structured (8) so that in the second etching step for the membrane and the connections are etched simultaneously (9) until the membrane reaches the desired thickness and the wafer is through-etched, establishing the connections. After sputtering aluminum on the top side, the nitride is removed through dry-etching and the bottom side was sputtered with aluminum, so that an electrical connection could be generated (10). The aluminum was then structured on the bottom side and the oxide and nitride layers were removed to enable anodic bonding.

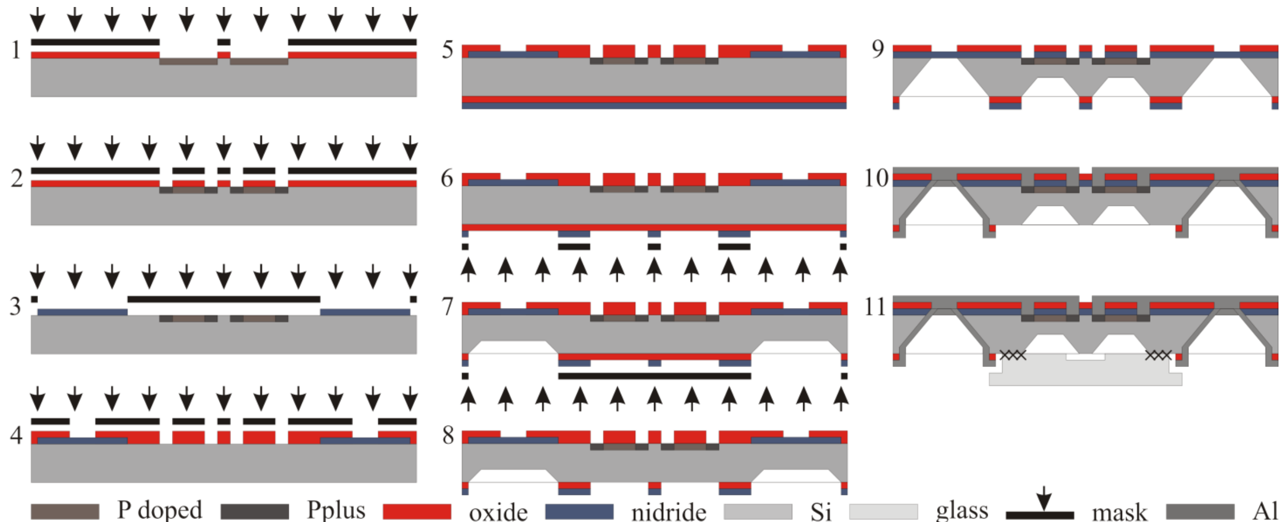

Figure 5: Most significant process steps including bonding (not in scale).

The glass cover was fabricated in a separate process. Here the glass is covered by a structured gold layer. The glass was then etched by a hydrofluoric acid solution. After the bonding process the wafers were diced, as explained in 3.2.1.

In the last step the sensor is fixed on the polyimide foil. Here a conductive adhesive, soldering paste or balls of solder can be used to fix the sensor and guarantee the electrical connection as well. Some experiments have been conducted and are continually being used to improve the pass rate.

3.2 Improvements

In this section the latest improvements towards the future goal of a robust high precision sensor are described. The main focus is on the pressure cavity under the membrane and the anodic bonding of the glass cover. Up to now, these covers have been glued manually piece by piece, because anodic bonding was not possible due to the through wafer connection. Also the high process temperature was thought to be problematic, because the pressure within the cavity under the membrane has a high impact on the range of p_o. Therefore several techniques were used to enable a free settable value p_i. This could increase the range and accuracy of the sensors.

3.2.1 Anodic Bonding

For anodic bonding of silicon and glass a bonder has to be used. The two wafers, which have been aligned properly to each other in advance, are placed within this machine. The chamber is then heated to temperatures in the range of 300 to 500 *°C*. A high DC potential of 50 to 1000 *V* has to be applied with an anode pressed on the top substrate to start the bonding process. Due to the electrical field and the elevated temperature a solid chemical bond between the substrates is created which is not reversible.

To enable the process, both substrates have to be in contact. No other layers, such as metals, silicon oxide or nitride may be at the positions where the substrates have to be bonded. The fabrication processes has to be improved for both parts: the sensor wafer and the glass wafer. The results are shown in Figure 6.

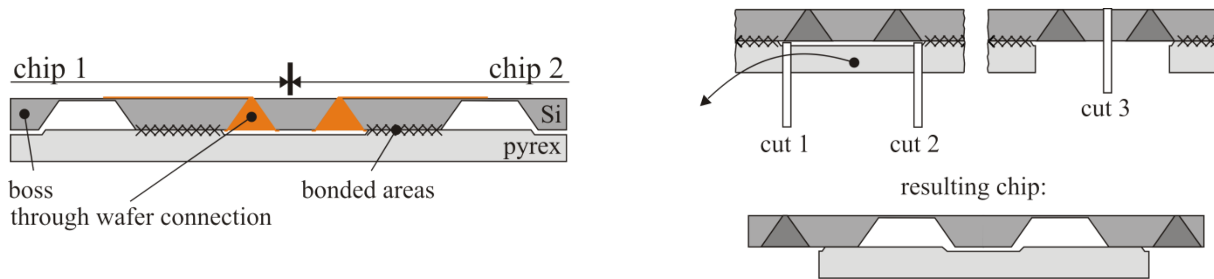

Figure 6: Drawing of the contact area between silicon and glass wafer (left) and the cutting steps needed for production (right).

The glass wafer is etched 4 µm at all positions where the silicon wafer has an overlap (see Figure 5). The results from the through wafer connection is presented in [6]. By cutting the wafers in a special order from bottom side, the chips obtain the desired contour. In this way, the required time and effort for the assembly is reduced significantly.

The bonding parameters were set to T=400 *°C*, V=400 *V* and $p_1=p_{ambient}$ for two hours. The high process temperature leads to undesired properties in the sensor, since the cavity is closed at a high temperature. Following the ideal gas law (4) a bonding process at ambient pressure p_1 and T_1=673.15 *K* leads to a pressure within the cavity of p_2=0.44 *bar* after cooling down the chip to ambient temperature T_2.

$$pV = nRT \Rightarrow \frac{p}{T} = \frac{nR}{V} = const. \Rightarrow \frac{p_1}{p_2} = \frac{T_1}{T_2} \tag{4}$$

To avoid this reduced cavity pressure p_i there are in principle three possibilities: Either, the pressure during the bonding process has to be increased, or the temperature has to be decreased. Unfortunately, a temperature reduction leads to poor bonding results. A pressure of 2.32 *bar* would be needed for compensation, which is technically not allowed in the bonder. The third possibility is to implement a channel to enable pressure balancing during cooling. Therefore different channels were designed and closed at room temperature. Some are shown in Figure 7.

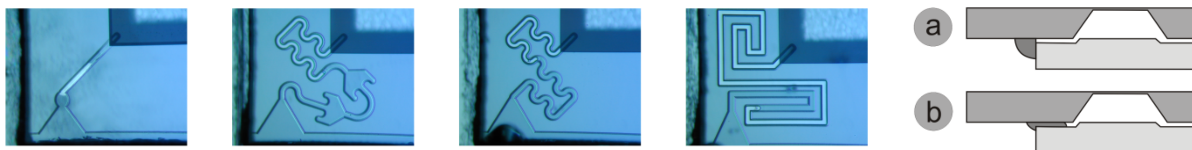

Figure 7: Four photos of different channel types leading into the cavity and principle of the sealing process.

After bonding and cutting the wafers, the 8 µm deep channels were filled with SU-8 50 photoresist. This negative resist was chosen because it has a high viscosity so it does not flow too deep into the cavity. The resist can be cured at 200 *°C* so it is able to withstand the planned embedding process. The application of the resist was conducted manually with a dispenser (Figure 7 a)). The resist then flows into the channel due to capillary action (Figure 7 b)). After approximately 1 min the flowing process stops. Although this process proved to be very time intensive, it was demonstrated successfully. The resist also did not flow into the membrane.

To reduce the time intensiveness, we carefully tried to operate the anodic bonding machine above the operating limits at 2.32 *bar*. The machine did not indicate any failures and the result was great. Additionally to the adaption of the process plan, the creation of a cavity via anodic bonding was demonstrated. The pressure can be individually set up to 2.32 *bar* during the bonding process, leading to a customized pressure at ambient temperature in the cavity. Therefore the range of the pressure sensor is raised, without any significant changes in the geometry or in the micro fabrication process.

3.2.2 Pressure chamber

For the first measurements with the custom made pressure sensors, a pressure chamber was designed. With this chamber automated tests are possible. It can be filled with water to simulate the real operating conditions mentioned in section 2.1.

The in-house air supply delivers dry and clean air at 8 *bar*. A precision proportional pressure regulating valve is used to control the pressure within the chamber. The valve has a 0 to10 *V* input and delivers a voltage signal in the same range as output proportional to the pressure. Therefore the actual pressure indicated by the valve can be measured. The valve has a maximum accuracy of ±50 *mbar* within the range of 0 to 6 *bar,* according to the manufacturers' information. A 16-bit DAQ System is used to control the valve as well as the sensor. At the connector block, five analog inputs are used to convert the output voltages of the four amplified sensor bridges and the valves' sensor. One analog output is used to provide the input voltage of the valve.

Inside the chamber the sensor is connected to a feedthrough, which is connected to a four channel signal amplifier outside. Furthermore the amplified sensors' signals are fed to four other analog inputs of the DAQ System. Figure 8 shows the simplified system set-up.

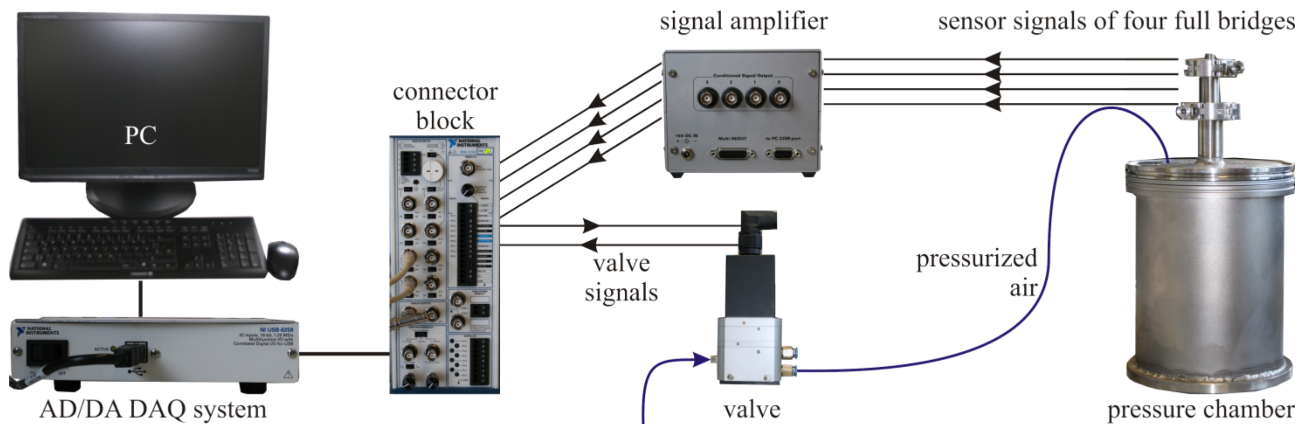

Figure 8: Simplified set-up of the calibration system including all components.

All measurements have been taken using this setup. The system currently operates at pressures up to 1.5 *bar*, which is the maximum approved pressure range of the feedthroughs. For future experiments, feedthroughs which are suitable for pressures up to 4 *bar*, are necessary to improve the performance.

4. RESULTS

In this section the results of the preliminary tests are presented.

4.1 First measurements

During the tests, the pressure in the chamber is altered stepwise using LabView© control software. In the software, different test cycles have been programmed. Mostly a stepwise pressure change is used, where the maximum and the minimum pressure can be regulated. Additionally, the amount of steps and the stabilization time can be adjusted. Due to the thin tubes and the relatively high volume of the chamber (ca. 8 *l*) it takes some time (<2 *s*) until the pressure in the chamber reaches the desired value given by the valve. After a short stabilization period the pressure becomes constant. The program then begins to acquire the sensor signals from the micro fabricated sensor as well as the valves' pressure sensor. Directly after the measurement, the pressure is changed to the next value, and the same routine at the new pressure step is performed. Figure 9 shows the difference between the valves' sensor signal p_{actual} and the given value

p_{given} over the given pressure p_{given}. It can be seen, that the actual value is constantly too low. For the measurements with our sensor we fitted the output voltage to the valve using the linear regression formula given in Figure 9 to get the pressure in the chamber closer to the desired pressure. In fact, it is not possible to raise the accuracy by doing so, because one does not know if the sensor or the valve is more exact. Due to correlation issues, it was determined, that the valves' sensor is more exact, than the valve itself. A reference sensor (0.01% accuracy full scale) has been purchased and will be used in the future to verify this assumption.

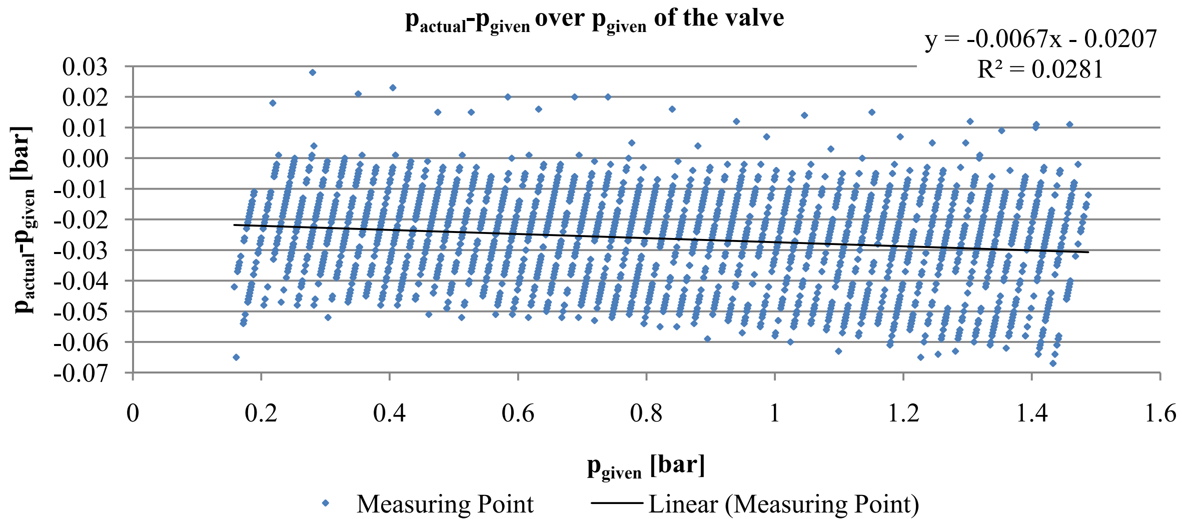

Figure 9: Valves' sensor signal p_{actual} minus the given pressure p_{given} over given pressure including a linear regression curve with its formula.

The manufacturer of the valve indicates the maximum accuracy of ±50 *mbar*. As one can see, the discrepancy is sometimes higher than this value. After the correction with the formula, only two of 3000 measurement points are outside this range, and the linear average is 0.

$$p_{actual,corr} = p_{actual} + 0.0067 \cdot p_{actual} + 0.0207 \quad bar \tag{5}$$

The next figure shows the amplified sensor signals over the actual pressure.

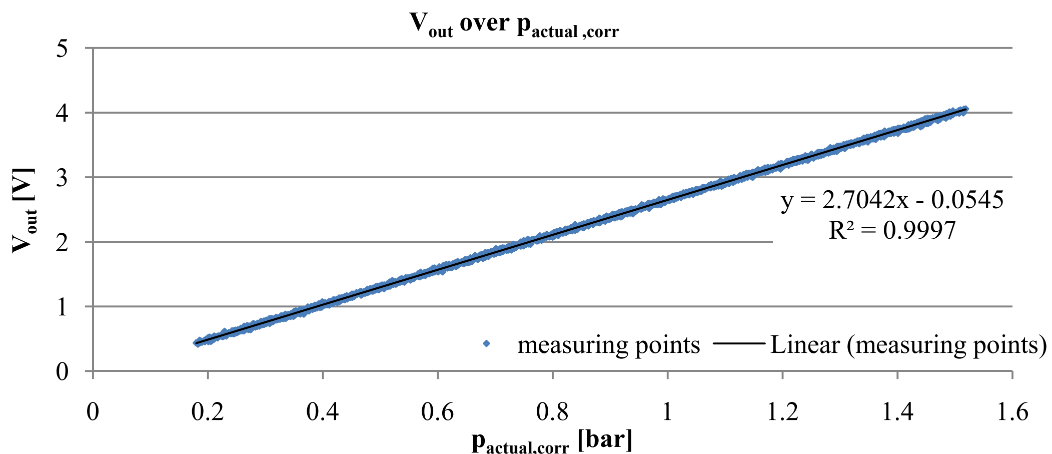

Figure 10: Signals from micro fabricated sensor (bridge 1) V_{Out} over corrected actual pressure $p_{actual,corr}$.

The formula given in the diagram is the transfer function. It does not represent the real output of the sensor, because an operational amplifier is used. Therefore, the slope has to be divided by the amplification factor and the voltage. The

offset has also been cancelled out by the signal conditioner. Unfortunately these data were not saved in the measurement file. Hence, a comparison between the real and the estimated sensitivity is not possible. The lag is already eliminated.

4.2 Linearity of the sensor

Another intension during the development was to create a sensor with a linear behaviour. Although the tests were performed in the range of 0 to 1.5 *bar,* and not until the absolute design limit, the results are promising. The next figure shows the difference between a linear regression of the output voltage $V_{Out,lin}$ and the actual value V_{Out} over the corrected pressure $p_{actual,corr}$.

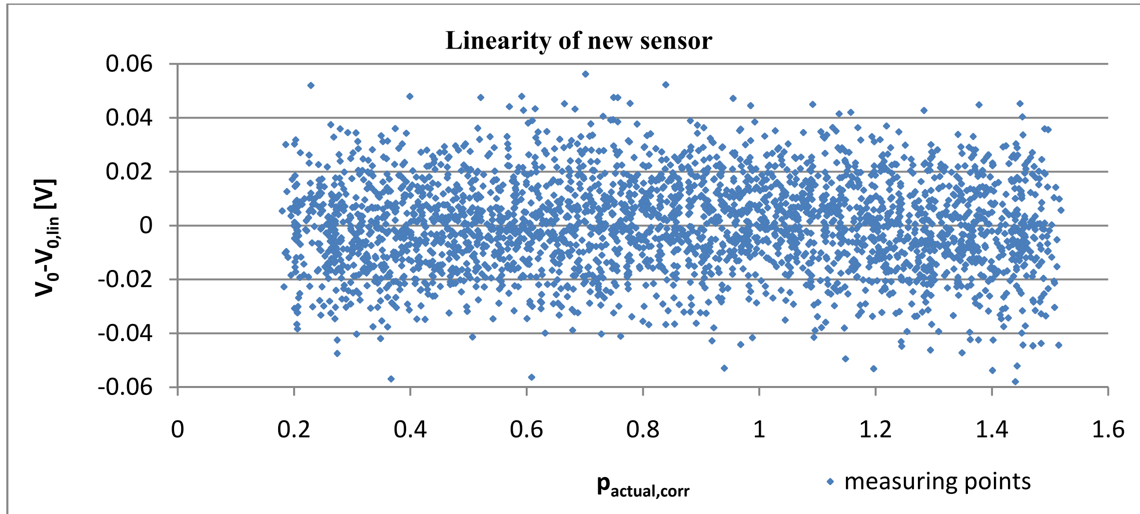

Figure 11: The difference of V_{Out} and the linear regression $V_{Out,lin}$ from micro fabricated sensor (bridge 1) over $p_{actual,corr}$.

Measuring a linear behaviour of our sensor at a pressure range of 0 to 1.5 *bar*, it can be assumed that the linearity remains constant until a pressure of 4 *bar*. In the current range, the maximum discrepancy of ±0.05 *V* complies with a pressure of 0.018 *bar*.

4.3 Time capability

Due to the membrane stiffness and the boss' mass, the eigenfrequency of the fabricated sensor has been simulated with CosmosWorks© and was found to be between $9.46 \cdot 10^9$ *rad/s* (=$1.51 \cdot 10^9$ *Hz*) and $9.08 \cdot 10^9$ *rad/s* (=$1.44 \cdot 10^9$ *Hz*). This frequency is much higher than the measuring frequency. This is limited by the amplifier and the DAQ system. The amplifier used has a bandwidth (-3*dB*) of 300 *kHz* per channel and the DAQ System has a sampling rate of 1 *MS/s* at 16-bit mode using more than one channel. Whether the amplifier or the DAQ System is the limiting component depends on the amount of channels used simultaneously. One DAQ system can handle three amplifier modules of that type. When using more, the DAQ System is the limiting factor. Tests are scheduled to find qualified values for the noise and temperature effects.

5. CONCLUSIONS & OUTLOOK

The first measurements with the newly installed set-up fulfil all expectations. The entire design and development process has resulted in a very linear and robust pressure sensor.

In the near future, the next steps will be to verify the sensors' sensitivity and the correct position of the piezoresistors. Therefore, the amplification factor and the offset correction introduced by the amplifier have to be determined. A comparison between the theoretical maximum sensitivity given in (4) and the measured sensitivity can be obtained. With new technical equipment, the pressure range of the chamber has to be increased to the desired maximum pressure in order to be able to measure the full span. Also, a reference sensor has to be installed in the chamber. To analyse thermal effects, an additional temperature sensor has to be applied in the chamber. Up to now, the temperature within the chamber has been unknown due to the pressurized air, which might cool the inside of the chamber during expansion.

Aside from the pressure sensor itself, related issues such as embedding working sensors with all implemented features into the fibre material have to be performed. Thereafter new tests are required to check if the embedding process has any influence on the sensors behaviour. In the future, a hot-wire anemometer will be integrated on the chip of the pressure sensor. The combination of pressure sensor and a hot-wire sensor is considered to be a promising development [4], [9], [10].

ACKNOWLEDGEMENTS

This work was funded by the German Research Foundation in the framework of the collaborative research centre 880 "Fundamentals of High Lift for Future Civil Aircraft". We would like to thank all our project partners for the cooperative and effective work.

REFERENCES

[1] Beutel, T., Leester-Schädel, M., Wierach, P., Sinapius, M. and Büttgenbach, S., "Novel Pressure Sensor for Aerospace Purposes", Sensors & Transducers Journal IFSA 115, Issue 4, ISSN 1726-5479, 11-19 (2010).

[2] Phataralaoha, A., Büttgenbach, S., "A novel design and characterization of a micro probe based on a silicon membrane for dimensional metrology", Proc. Eurosensors XIX 2005, WPb31 (2005).

[3] von Papen, T., Buder, U., Ngo, H., Obermeier, E., "A second generation MEMS surface fence sensor for high resolution wall shear stress measurement", Sensors and Actuators A 113, no. 2, 151-155 (2004).

[4] Ebefors, T., Kälvesten, E., Stemme, G., "Three dimensional silicon triple-hot-wire anemometer based on polyimide joints", Proc. of the Eleventh Annual International, 93-98 (1998).

[5] Buder, U., Henning, L., Neumann, A., Obermeier, E., "Aeromems Wall Hot-Wire Sensor Arrays on Polyimide with Through Foil Vias and Bottom Side Electrical Contacts", Proceedings of Transducers 2007, 3E02.P 2007.

[6] Triltsch, U., Büttgenbach, S., "Next Generation of TCAD Environments for MEMS Design", DTIP of MEMS/MOEMS, (2008).

[7] Beutel, T., Ferreira, N., Balck, A., Leester-Schädel, M., Büttgenbach, S. "Cell Manipulation System Based on a Silicon Micro Force Sensor with Self-Calibration from Backside", Proc. IEEE Sensors 2010, (ISBN 978-1-4244-8168-2), 1419-1423 (2010).

[8] Leester-Schädel, M., Beutel, T. ,Büttgenbach, S., "Entwicklung eines Herstellverfahrens für die rückseitige, elektrische Kontaktierung von mikrotechnischen Membran-Sensorelementen", MST Kongress, 746-749 (2009).

[9] Schiffer, M., Obermeier, E., Grewe, F., Ebner, A., Fernholz, H.H., "A new height-adjustable aeroMEMS surface fence probe fabricated in SOI technology for high resolution wall shear stress measurement in turbulent flows", Transducers 2005, Digest of Technical Papers, 601-604 (2005).

[10] Berns, A., Buder, U., Wang, X. H., Nitsche, W., Obermeier, E., "AeroMEMS pressure sensor with integrated wall hot-wire", Proc. IEEE Sensors 2008, 5L-B1 (2008).